A comparison of surface preparation techniques for wind turbine field repairs

IOP Conf. Series: Materials Science and Engineering **942** (2020) 012012 doi:10.1088/1757-899X/942/1/012012

A comparison of surface preparation techniques for wind turbine field repairs

Ariel Lusty*, Douglas Cairns, David Miller, and Daniel Samborsky

Department of Mechanical and Industrial Engineering, Montana State University, Bozeman, MT, 59715, USA

*Corresponding author's email: arilusty@gmail.com

Abstract. Wind turbine service lifetimes can exceed 20 years. This extreme operational demand necessitates reliable and consistent field repairs; however, the effects of current wind turbine field repair surface preparation techniques are not well-documented and are thus not well-understood. This leads to reliance on technician experience rather than scientific data for repair procedures, which causes variability in the quality of repairs. Solvent wiping is a common procedure for contaminant removal after damaged material is removed from a wind turbine blade, but it was unknown if solvent wiping reduced the surface energy and consequently the likelihood of a durable repair. The goal of this study was to quantify the effects that various surface preparation techniques have on the overall strength and reliability of wind turbine repairs. Type of reagent-grade solvent, fiber direction, matrix, and adhesive were varied for contact angle, lap shear, Double Cantilever Beam (DCB), and End-Notch Flexure (ENF) testing. The type of solvent used did not affect surface energy, maximum lap shear stress, or modes I and II fracture toughness values. However matrix-adhesive combinations significantly affected maximum lap shear stress and fracture toughness values.

1. Introduction

Fixing structural damage is of utmost priority for owners and operators of wind turbines. Structural damage is typically from manufacturing defects, but may include in-service damage from mechanical fatigue, bird collisions, or lightning strikes. Damage that inhibits a wind turbine from efficiently harvesting energy should be repaired if the repair does not exceed the cost of blade replacement or if the procedure is economically viable for other reasons. The goal of any repair is to return the structure to its original strength, stiffness, shape, and surface finish [1]. The most common and preferred structural wind turbine blade repair method is the scarf repair due to the need to restore strength, avoid load concentration and eccentricities, and maintain aerodynamic efficiency.

Regardless of the repair design, contamination will be present before, during, and after damage removal. A commonly used technique for contaminant removal involves wiping a surface with reagent grade solvents to remove contamination and wiping again with a dry cloth to remove the solvent before it evaporates. It is essential to ensure that the solvent being used is capable of dissolving the contaminant without further damaging the composite structure [2]. If the use of solvents damages the surface of the composite structure, bond strengths and repair durability could be compromised.

In this research, the effects of current solvent wiping techniques on composite bond strengths were investigated using direct adhesion measurements and surface characterization techniques [3]. Direct adhesion measurements are destructive methods that measure the force required to break, tear and delaminate surfaces at the interface. Direct adhesion measurements used in this study were lap shear, DCB, and ENF tests. Understanding failure initiation and propagation through failure surface examination is crucial after direct adhesion measurements, so adhesive failure modes were documented for each direct adhesion measurement. Four adhesive failure modes were considered: interfacial failure,

cohesive failure, stock-break failure, or fiber-tear failure. Interfacial failure occurs along the adhesive-substrate interface and is usually due to a lack of chemical bonding. Cohesive failure occurs within the adhesive and is typically the preferred type of failure in a bonded joint because cohesive failure usually corresponds with a higher maximum lap shear stress. Stock-break failure occurs when the substrate is either damaged or weaker than the adhesive bond. Fiber-tear failure occurs when the top layer of the substrate is damaged, resulting in fiber re-exposure.

Vacuum assisted resin transfer molding (VARTM) was used to manufacture glass fiber reinforced polymer (GFRP) composite substrates. Sessile drop contact angle testing was used for surface characterization, and was conducted after composite samples were sanded and wiped with reagent grade solvents including acetone, methyl ethyl ketone (MEK), methyl isobutyl ketone (MIBK), or isopropyl alcohol (ISP), as these are commonly used solvents in composite repairs [1]. Contact angle testing was also conducted on plasma-treated specimens, as plasma treatment is a common method used to increase surface energy [4].

Lap shear, DCB, and ENF testing using two different adhesives was used to compare the effects of wiping substrate surfaces with different solvents on resulting maximum lap shear stress, mode I fracture toughness (G_{IC}), and mode II fracture toughness (G_{IIC}) values. Dillingham demonstrated using DCB testing that cohesive failure corresponded with higher G_{IC} values, and interfacial failure corresponded with lower G_{IC} values [5]. Overall, if a solvent had deleterious effects on bond strength more than another, it would be reflected in differences in contact angles, lap shear strengths, G_{IC} values, G_{IIC} values and adhesive failure modes.

2. Materials

Materials were selected to replicate the surfaces that would be encountered in a wind turbine blade field repair. Wind turbine blade face sheets are often manufactured using both 0° and ±45° glass fibers, with either an epoxy or a vinyl ester matrix. Accordingly, VARTM was used to make $[0]_4$ epoxy, $[45]_6$ epoxy, $[45]_6$ vinyl ester, and $[0]_4$ vinyl ester composites for contact angle and lap shear testing. VARTM was also used to make $[0]_6$ epoxy and $[0]_6$ vinyl ester specimens for DCB and ENF testing. Unidirectional Vectorply E-LT-2900 fabric was used for unidirectional layups, and ±45° PPG D810 fabric was used for $[45]_6$ layups. Hexion Epikote MGS RIMR 135 epoxy was used for the epoxy composites, and Fibreglast 1110 vinyl ester resin was used for the vinyl ester composites. Two adhesives were compared in lap shear, DCB, and ENF testing: Huntsman Araldite 2051 and Loctite EA 9396 Aero. Huntsman Araldite 2051 is a methyl methacrylate adhesive, and Loctite EA 9396 Aero is an epoxy adhesive. Wypall X60 cloths were used for solvent wiping.

3. Experimentation

3.1 Solvent Wipe Contact Angle Tests

Sessile drop contact angle testing can be used to calculate surface energy, which is the work spent in forming a unit area of a solid surface. Contact angle testing involves the placement of a water droplet on a surface and measuring the resultant angle the droplet makes with the surface. Low contact angle values correspond with hydrophilicity, high wettability, and higher surface energy. Alternatively, high contact angles indicate hydrophobicity, low wettability and lower surface energy [6]. Additionally, low surface energy has been shown to result in more interfacial failure modes, and high surface energy will typically result in more cohesive failure modes [5].

Sessile drop contact angle testing was conducted after samples were sanded and wiped with solvents. For contact angle testing, 25 x 50 mm^2 samples were first wet sanded using Federation of European Producers of Abrasives (FEPA) 1000 grit sandpaper, then wiped with a dry cloth to remove water. The water break test was used to ensure mold release was removed from composite surfaces [7]. Next, the samples were wiped with another cloth that had been saturated with either distilled water, ISP, acetone, MIBK, or MEK. Then, samples were wiped with a dry cloth. Six contact angle tests were conducted on the surface of each sample.

Contact angle testing was conducted immediately after solvent wiping. A 1 µL droplet of MilliQ 0.2 µm water was formed at the tip of the needle. Next, the substrate was slowly brought up to the droplet.

Once the droplet contacted the surface, the substrate was lowered. The contact angle decreases linearly with time after a water droplet is placed on a surface. Conclusions from preliminary testing demonstrated that water droplets would stabilize, but not completely evaporate, after approximately 10 seconds. Thus, after the droplet was on the composite surface for 10 seconds, an image was captured using VCA Optima software. Contact angles were also measured using VCA Optima.

3.2 Plasma Contact Angle Tests

Specimens cut from the same composite plates as the solvent wipe contact angle tests were shipped to Enercon Industries Corporation for plasma treatments, followed immediately by contact angle testing. Specimens were sanded with FEPA 1000 grit sandpaper prior to shipment to remove mold release. Two areas on each sample were contact angle tested before and after being treated by two surface treatment types: a blown ion treatment and a flame treatment. The line speed was run at 30.5 cm per minute for both blown ion and flame treatments. The output used for the blown ion treatment was at 0.5 kW, and the output for the flame burner was 200 liters per minute. The distance between the blown ion treatment and the sample was 6.35 mm, and the distance between the flame treatment and the sample was 50.8 mm.

3.3 Lap Shear Tests

In addition to contact angle tests, lap shear tests were used to compare the effects of solvent wipe techniques on the resulting maximum lap shear stress values and lap shear failure modes. It is important to note that lap shear testing does not produce true ultimate stress because the stress distribution in the adhesive is not uniform over the bond area [8]. Additionally, the stiffness of adherends influences peel stress concentrations at the end of the joint in lap shear testing. Increasing the modulus or thickness of adherends will lead to an increase in apparent strength of the bond. Nevertheless, lap shear data does have value from a comparative standpoint and was thus used to check the effectiveness of different surface preparation techniques [9].

Coupons with dimensions 25 x 400 mm^2 were cut from composite plates. Instead of the FEPA 1000 sand grit that was used for contact angle testing, FEPA 320 grit sandpaper was used to create a rougher surface and to promote adhesion for lap shear testing. Solvent wipe techniques identical to those used in contact angle testing were used prior to adhesive bonding. Wire with a 0.33 mm diameter was placed in tab areas as spacers, and weights were used to reduce variation in adhesive thicknesses. The maximum lap shear stress is reported as the failure stress in the adhesive, which is found by dividing the failure load by the bond area. The $[45]_6$ laminates were tested at 13 mm/min load rate to minimize creep, and $[0]_4$ laminates were tested at 1 mm/min load rate [10]. No significant differences in maximum lap shear stress were found between the two load rates. The failure surfaces of each lap shear specimen were visually inspected and assigned failure mode types.

3.4 DCB Tests

Similarly to the lap shear tests, coupons were cut to dimensions 25 x 400 mm^2 and FEPA 320 grit sandpaper was used to hand-sand samples on a flat granite surface plate. Solvent wipe techniques identical to those used in contact angle testing were used prior to adhesive bonding. In addition, the same two adhesives from lap shear testing were used to adhere coupons together. Teflon films were used as starter cracks and were placed at the ends of the specimens. Unlike for lap shear specimen preparation, wire spacers were not used for DCB specimen preparation. Instead, binder clips were used to secure coupons together while adhesives cured. After adhesives were cured, all edges of each specimen were trimmed and polished. Aluminum tabs were adhered to specimens using Plexus MA310 methacrylate adhesive. DCB specimens were tested in tension at a loading rate of 0.3 mm/sec. Data was acquired using HP Logger software. G_{IC} was calculated from [11]. Values of 40270 MPa and 125 MPa were used for E_{11} and E_{22}, respectively, and were found using [12]. P was found using the 5% rule, which involves finding the slope of the force-displacement curve generated in DCB tests, then taking 95% of the slope and using the load where the 95%-of-the-slope line intersects plotted data points. The 5% rule is a common approximation used to account for the nonlinearity in DCB test data [13].

3.5 ENF Tests

Post-tested DCB specimens were used for ENF tests. Cracks from the DCB specimens were manually propagated and remeasured because a longer crack was necessary for ENF testing to avoid local face sheet delamination from the loading nose. Specimens were placed in the loading fixture such that the crack tip was approximately halfway between the supporting roller and the loading roller. G_{IIC} was calculated using an equation from [11]. The compliance term in [11] was not needed in calculations for this study because DCB and ENF tests were conducted separately, rather than with a mixed-mode bending apparatus. The E_{11} value from DCB tests was used. Shear modulus G_{13} (5050 MPa) was found using Iosipescu notched-shear tests and digital image correlation (DIC) [14]. After Iosipescu tests, GOM-ARAMIS software was used to calculate strain. The surface component used was based on a facet size of 25 and a point distance of 17. A spatial average filter of 2 was used. After ENF tests, specimens were manually peeled apart and, similarly to after lap shear tests, adhesive failure modes were identified for DCB and ENF failure surfaces.

4. Results and Discussion

4.1 Solvent Wipe Contact Angle Results

Results for contact angle testing after wiping with solvents are summarized in Table 1. The *unprepared* samples were neither sanded nor solvent wiped, so mold release was still present on the surfaces. The *dry wipe* samples were wet sanded and wiped with dry cloths before contact angle testing.

Table 1. Average contact angle (degrees) for each surface treatment.

Treatment	$[0]_4$ Epoxy	$[45]_6$ Epoxy	$[0]_4$ Vinyl Ester	$[45]_6$ Vinyl Ester
Unprepared	87.7 ± 3.5	73.4 ± 5.0	87.8 ± 9.6	70.6 ± 12.8
Dry Wipe	64.3 ± 5.4	66.8 ± 9.7	67.1 ± 6.8	67.6 ± 6.3
Distilled Water	56.5 ± 5.9	79.0 ± 2.1	59.5 ± 9.9	82.1 ± 5.6
ISP	59.4 ± 5.4	70.2 ± 6.4	65.0 ± 9.1	72.0 ± 6.7
Acetone	54.5 ± 7.2	73.0 ± 2.6	67.3 ± 9.4	68.1 ± 3.7
MIBK	62.3 ± 6.1	58.7 ± 6.4	61.1 ± 5.2	71.8 ± 3.7
MEK	62.4 ± 7.3	65.5 ± 8.5	60.9 ± 8.9	68.3 ± 5.8

The contact angle was neither significantly altered by wiping samples' surfaces with solvents, nor the type of matrix used. However, removing mold release through sanding is necessary to decrease the contact angle, as shown in the drops in contact angle between *unprepared* and solvent wiped samples in the $[0]_4$ epoxy and vinyl ester columns.

4.2 Plasma Treatment Contact Angle Results

Contact angles across all solvent-wiped specimens were high, indicating poor wettability and poor adhesion. To decrease contact angle, samples were plasma treated followed by contact angle testing.

Table 2. Average contact angles and standard deviations on composite surfaces before and after blown ion treatment.

Treatment	$[0]_4$ Epoxy	$[45]_6$ Epoxy	$[0]_4$ Vinyl Ester	$[45]_6$ Vinyl Ester
Initial (before blown ion treatment)	73.5 ± 0.2	71.1 ± 0.7	75.0 ± 3.7	70.4 ± 3.7
After blown ion treatment	30.2 ± 2.2	30.6 ± 2.3	16.2 ± 0.0	22.9 ± 0.8

Across all composite surface types in Table 2, there was a 66% drop between the average contact angles before and after blown ion treatment.

Table 3. Average contact angles and standard deviations on composite surfaces before and after flame treatment.

Treatment	$[0]_4$ Epoxy	$[45]_6$ Epoxy	$[0]_4$ Vinyl Ester	$[45]_6$ Vinyl Ester
Initial (before flame treatment)	70.2 ± 0.1	78.5 ± 2.5	63.5 ± 0.2	77.7 ± 1.3
After flame treatment	25.8 ± 0.4	28.9 ± 0.9	15.9 ± 0.4	18.8 ± 2.5

Across all composite surface types in Table 3, there was a 69% drop between the average contact angles before and after flame treatment. Overall, contact angle dropped significantly between initial and plasma treated composite surfaces for both blown ion and flame treatments, indicating that wettability and adhesion properties were improved.

4.3 Lap Shear Results

The moduli of the $[0]_4$ and $[45]_6$ adherends were 39.4 and 13.3 GPa, respectively. Lap shear test results for the Huntsman Araldite 2051 adhesive are shown in Table 4. Figures 1, 2, and 3 include common fracture surfaces for lap shear tests for each adhesive. Lap shear test results for the Loctite EA 9396 Aero adhesive are shown in Table 6. Five test results were averaged for each tabulated value.

Table 4. Average maximum lap shear stress (MPa) and standard deviations for specimens adhered with a 658 ± 19 mm^2 average bond area of Huntsman Araldite 2051.

Surface Treatment	$[0]_4$ Epoxy	$[45]_6$ Epoxy	$[0]_4$ Vinyl Ester	$[45]_6$ Vinyl Ester
Sanded	14.89 ± 0.77	6.89 ± 0.29	22.61 ± 1.56	7.69 ± 0.63
ISP	14.52 ± 0.55	7.31 ± 0.58	22.17 ± 1.45	6.57 ± 0.93
Acetone	13.67 ± 2.33	6.88 ± 0.78	22.80 ± 0.46	8.48 ± 0.48
MIBK	14.13 ± 1.38	6.99 ± 0.94	22.75 ± 1.65	7.96 ± 0.13
MEK	13.49 ± 2.14	6.83 ± 1.21	23.63 ± 0.86	8.07 ± 0.38

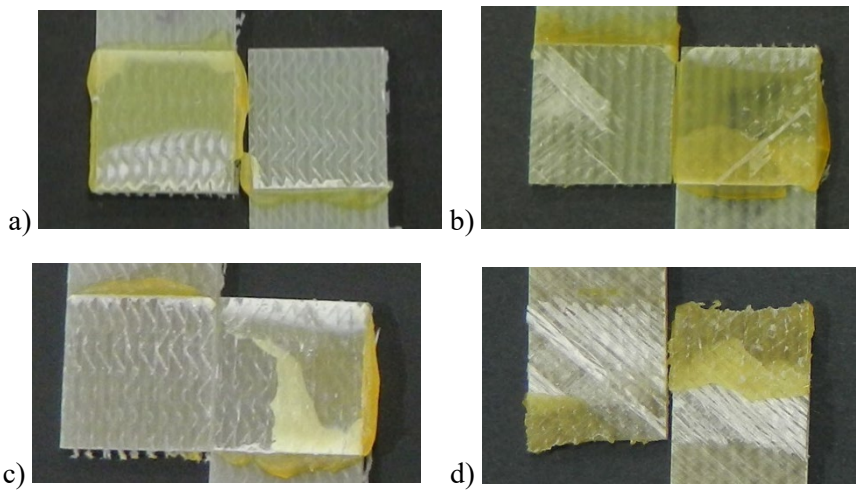

Figure 1. Huntsman Araldite 2051 adhesive fracture surface photographs showing the primary failure modes for each substrate type: a) $[0]_4$ epoxy substrates (ISP wipe) with interfacial failure mode; b) $[45]_6$ epoxy substrates (MIBK wipe) with fiber-tear failure mode; c) $[0]_4$ vinyl ester substrates (ISP wipe) with interfacial failure mode; d) $[45]_6$ vinyl ester substrate (MEK wipe) with fiber-tear failure mode.

In contrast to Figure 1c with ISP wipe, the fracture surfaces in Figure 2 with MEK wipe show more cohesive failure.

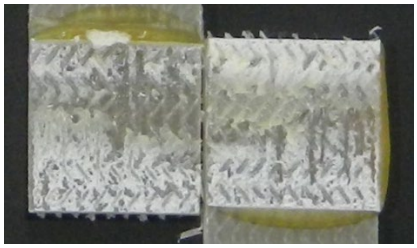

Figure 2. Primary failure mode for $[0]_4$ vinyl ester specimens wiped with MEK.

The $[0]_4$ vinyl ester specimens had higher maximum lap shear stresses than the $[0]_4$ epoxy specimens, while the epoxy and vinyl ester $[45]_6$ specimens all had around the same maximum lap shear stresses. There were no significant differences in maximum lap shear stress values from using different solvents. The $[0]_4$ specimens resulted in mostly interfacial failure, and the $[45]_6$ specimens had mostly fiber-tear failure. Although most $[0]_4$ vinyl ester specimens exhibited interfacial failure modes, those wiped with MEK exhibited the most instances of cohesive failure modes but did not have significantly higher maximum lap shear stresses. The $[0]_4$ specimens resulted in higher maximum lap shear stresses and $[45]_6$ layups resulted in the lowest maximum lap shear stresses. The $[45]_6$ specimens failed at lower ultimate tensile stresses than the $[0]_4$ specimens due to their higher susceptibility to bending in tension. Overall, the layup-matrix combinations had the most differences in resulting maximum lap shear stresses.

Table 5. Average maximum shear stress (MPa) for specimens adhered with a 658 ± 16 mm^2 average bond area of Loctite EA 9396 Aero Adhesive.

Surface Treatment	$[0]_4$ Epoxy	$[45]_6$ Epoxy	$[0]_4$ Vinyl Ester	$[45]_6$ Vinyl Ester
Sanded	13.84 ± 0.82	8.12 ± 0.47	5.81 ± 0.26	4.62 ± 0.50
ISP	13.05 ± 0.91	8.23 ± 0.30	6.56 ± 0.48	5.67 ± 0.32
Acetone	12.54 ± 0.27	8.16 ± 0.19	5.40 ± 0.28	4.96 ± 0.62
MIBK	13.39 ± 0.72	8.21 ± 0.14	5.63 ± 0.61	4.94 ± 0.48
MEK	12.62 ± 0.60	8.24 ± 0.11	5.81 ± 0.47	4.77 ± 0.34

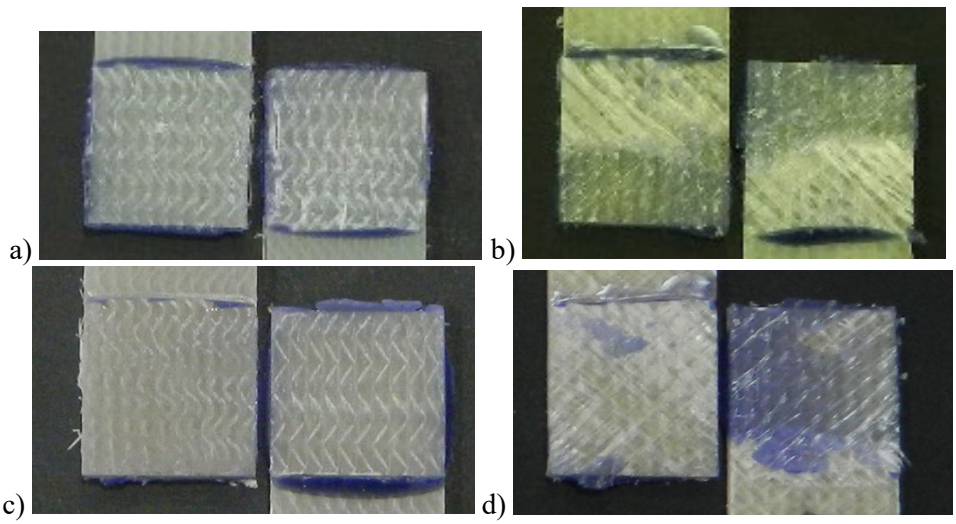

Figure 3. Loctite EA 9396 Aero adhesive fracture surface photographs showing the primary failure modes for each substrate type: a) $[0]_4$ epoxy substrates (ISP wipe) with cohesive failure; b) $[45]_6$ epoxy substrates (MEK wipe) with fiber-tear failure; c) $[0]_4$ vinyl ester substrates (acetone wipe) with interfacial failure; d) $[45]_6$ vinyl ester substrates (MIBK wipe) with fiber-tear failure.

When using the Loctite EA 9396 Aero adhesive, the $[0]_4$ epoxy specimens had the highest maximum lap shear stresses and the vinyl ester specimens had the lowest maximum lap shear stresses. The Loctite EA 9396 Aero epoxy adhesive likely has a more similar molecular structure to the epoxy matrix than the vinyl ester matrix, which could explain why maximum lap shear stresses were higher than with the $[0]_4$ vinyl ester specimens. The $[0]_4$ epoxy specimens resulted in mostly cohesive failure, while the $[45]_6$ epoxy and $[45]_6$ vinyl ester specimens resulted in mostly fiber-tear failure.

4.4 DCB and ENF Test Results

Mode I and mode II fracture toughness values are presented, and DCB and ENF failure modes are discussed. DCB and ENF results for the Huntsman Araldite 2051 adhesive are in Table 6, and DCB and ENF results for the Loctite 9396 Aero adhesive are in Table 7. Five test results were averaged for each tabulated value. Figure 3 is an example of DCB load-displacement curves for specimens wiped with acetone.

Table 6. Modes I and II fracture toughness values for glass fiber reinforced epoxy and vinyl ester substrates adhered with the Huntsman Araldite 2051 adhesive.

	Epoxy Substrates		**Vinyl Ester Substrates**	
Surface Treatment	**G_{IC} (J/m^2)**	**G_{IIC} (J/m^2)**	**G_{IC} (J/m^2)**	**G_{IIC} (J/m^2)**
Sanded	390 ± 222	8079 ± 2143	553 ± 222	4468 ± 1821
ISP	605 ± 26	9170 ± 1297	426 ± 417	5425 ± 3581
Acetone	551 ± 203	10235 ± 3664	590 ± 168	2537 ± 1036
MIBK	583 ± 97	6601 ± 2630	867 ± 408	4621 ± 3443
MEK	602 ± 104	7079 ± 1780	702 ± 310	2209 ± 322

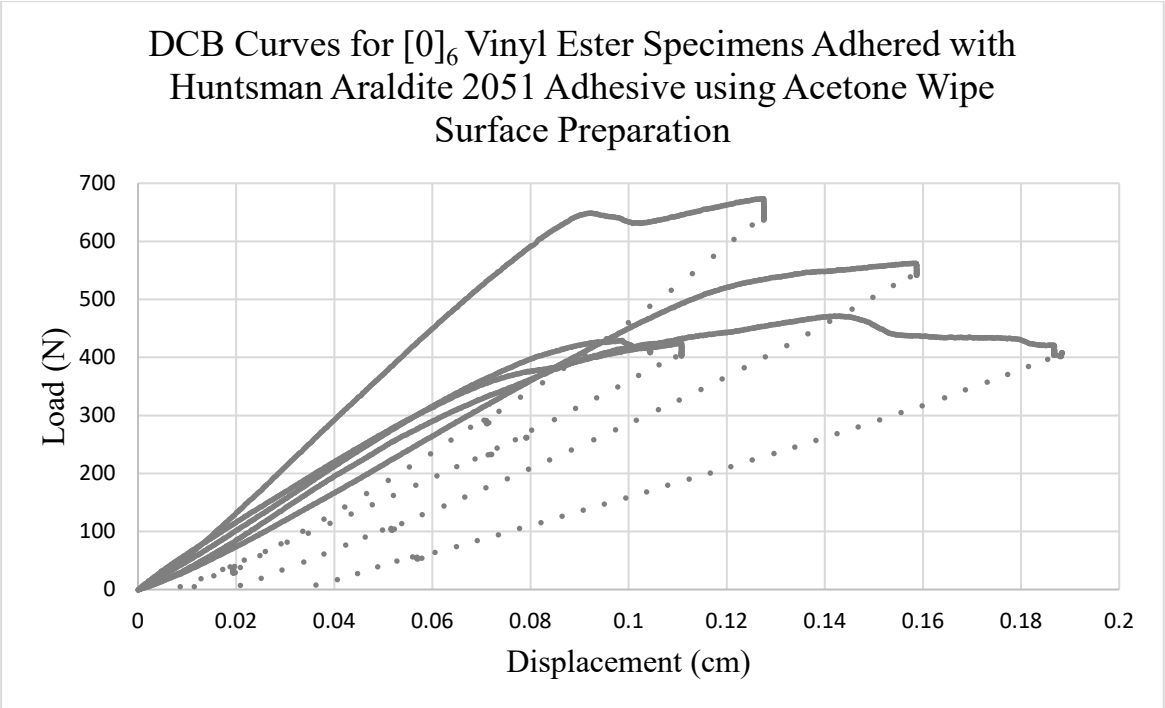

Figure 4. An example of five load-displacement curves from DCB tests.

There were no significant differences in G_{IC} or G_{IIC} values between surface treatment types for neither the epoxy nor the vinyl ester composites adhered together with the Huntsman Araldite 2051 adhesive.

Standard deviations were large for two reasons. First, even when using a flat granite sanding plate, hand sanding can result in surface variations from inevitable uneven pressure applied. Second, variations may also be due to complex stress distributions in adhesive layers. Crack and damage growth do not always occur in a simple and predictable fashion, which was observed in post-test crack length measurements and failure surface observations [15]. DCB tests for epoxy substrates resulted primarily in cohesive failure modes and ENF tests resulted in primarily interfacial failure modes. Both DCB and ENF tests resulted primarily in cohesive failure modes for vinyl ester specimens adhered with Huntsman Araldite 2051 adhesive.

Table 7. Modes I and II fracture toughness values for glass fiber reinforced epoxy coupons adhered together with Loctite EA 9396 Aero adhesive.

Surface Treatment	G_{IC} (J/m^2)	G_{IIC} (J/m^2)
Sanded	234 ± 72	2772 ± 269
ISP	166 ± 47	2418 ± 523
Acetone	149 ± 42	2930 ± 661
MIBK	157 ± 48	2173 ± 468
MEK	227 ± 83	2943 ± 1115

There were no significant differences in G_{IC} or G_{IIC} values between surface treatment types for epoxy coupons adhered together with Loctite EA 9396 Aero adhesive. Overall, epoxy coupons adhered together with Loctite EA 9396 Aero adhesive resulted in cohesive failure for both DCB and ENF tests. All glass fiber reinforced vinyl ester specimens adhered together with Loctite EA 9396 Aero adhesive, regardless of surface treatments tested, resulted in G_{IC} = 0 J/m^2. This result indicates that the Loctite EA 9396 Aero adhesive was incompatible with the vinyl ester composite substrate. ENF results were not collected for vinyl ester specimens adhered together with Loctite EA 9396 Aero adhesive. All G_{IC} values were lower than G_{IIC} values because cracks typically spread preferentially in a direction perpendicular to tensile stresses [16]. Epoxy substrates adhered with the Loctite EA 9396 Aero adhesive resulted in significantly lower G_{IC} and G_{IC} values compared to the Huntsman Araldite 2051. Overall, the vinyl ester substrates adhered with the Huntsman Araldite 2051 adhesive resulted in the highest G_{IC} values, and the epoxy substrates adhered with the Huntsman Araldite 2051 adhesive resulted in the highest G_{IIC} values.

5. Conclusions

Generally, wiping a composite substrate with either distilled water, ISP, Acetone, MIBK, or MEK does not significantly affect the resulting water contact angle, maximum lap shear stress, G_{IC} or G_{IIC} values. Contact angle testing demonstrated the importance of removing mold release from composites prior to bonding, and plasma treatment delivered promising results for decreasing contact angle but may be challenging to implicate into wind turbine field repairs due to already-present challenges with wind turbine blade accessibility. Furthermore, future work will examine the effectiveness of applying sizing to the surface of a composite in increasing resultant repair bond strengths.

Differences observed when testing different lap shear substrates were mostly due to differences in adherend thicknesses and moduli rather than the type of solvent used, which is expected because the stiffness of adherends influences peel stress concentrations at the end of the joint in lap shear testing. Adhesive-matrix combination also had a significant effect on the maximum lap shear stresses. Unidirectional vinyl ester lap shear specimens resulted in more cohesive failure when wiped with MEK than for those wiped with other solvents, but corresponding maximum lap shear stresses were not significantly higher. In addition, failure modes after DCB and ENF testing for MEK-wiped vinyl ester specimens adhered with methyl methacrylate were not visibly different. Even so, the causes for the increases in cohesive failure modes for the MEK-wiped vinyl ester substrates adhered with the methyl methacrylate adhesive merit further investigation.

Across all DCB and ENF tests, G_{IIC} values were consistently higher than G_{IC} values, which is optimal for wind turbine field repairs, particularly scarf repairs, because patches are typically subjected to more

shear stresses than peel stresses. Data from DCB and ENF tests may be used in modelling software such as ABAQUS to simulate repairs with the composite-adhesive combinations used in this study. SEM will be used in future work to confirm visually observed lap shear, DCB and ENF failure modes. Similarly to lap shear results, adhesive-matrix combinations had significant effects on G_{IC} and G_{IIC} values and on failure modes. G_{IIC} values for specimens adhered using the Huntsman Araldite 2051 adhesive were twice as high for the epoxy specimens than the vinyl ester specimens. Both epoxy and vinyl ester specimens had similar G_{IC} values when adhered with the Huntsman Araldite 2051 adhesive. Most notably, vinyl ester composite substrates adhered extremely poorly to the Loctite EA 9396 Aero adhesive, with no adhesive-matrix compatibility in mode I loading. Based on maximum lap shear stress values, vinyl ester composite substrates adhered with the Loctite EA 9396 Aero adhesive may have some shear strength, but since $G_{IC} = 0$ J/m^2, the Loctite EA 9396 Aero adhesive should be considered unsuitable for repairs to Fibreglast 1110 vinyl ester composites.

Additional testing using different adhesives and the effects of common contaminants and surface treatments using direct adhesion measurements and surface characterization techniques will be conducted in future work. Procedures will then be developed for the evaluation of solvent effects on composite surfaces, the evaluation of the effectiveness of solvents on the removal of common contaminants, and the evaluation of surface treatment effectiveness on increasing repair bond strength and durability. The development of these procedures is crucial to the advancement of wind turbine blade repair technology and thus the extension of wind turbine blade lifetimes.

References

[1] Dorworth L C 2013 Repairs for Advanced Composite Structures Automotive Composites Conference and Exhibition (Reno: Abaris Training)
[2] Dorworth L C, Gardiner G L and Mellema G M 2015 Essentials of Advanced Composite Fabrication and Repair (Newcastle: Aviation Supplies & Academics)
[3] Awaja F, Gilbert M, Kelly G, Fox B and Pigram P J 2009 Adhesion of Polymers *Prog. Polym. Sci.* vol 34 no 9 pp 948–68 DOI: https://doi.org/10.1016/j.progpolymsci.2009.04.007
[4] Mattox D M 2010 Substrate ('Real') Surfaces and Surface Modification (PVD) Processing Elsevier pp 25–72 DOI: https://doi.org/10.1016/b978-0-8155-2037-5.00002-2
[5] Dillingham R G and Oakley B R 2006 Surface Energy and Adhesion in Composite–Composite Adhesive Bonds *J. Adhes.* vol 82 no 4 pp 407–26 DOI: 10.1080/00218460600683944
[6] Erbil H Y 2006 Surface Chemistry of Solid and Liquid Interfaces (Oxford: Blackwell Publishing Ltd)
[7] Hart-Smith L J, Ochnsner R W and Radecky R L 1990 Surface Preparation of Composites for Adhesive-Bonded Repair *Engineered Materials Handbook: Adhesives and Sealants* (Cleveland: ASM International)
[8] Campbell F C 2004 Manufacturing Processes for Advanced Composites (New York : Elsevier)
[9] Duncan B and Crocker L 2001 Review of Tests for Adhesion Strength (Teddington : National Physics Laboratory Materials Centre)
[10] ASTM International 2014 ASTM D5868-01: Standard Test Method for Lap Shear Adhesion for Fiber Reinforced Plastic (FRP) Bonding DOI: 10.1520/D5868-01R14
[11] Reeder J R and Crews J H 1990 Mixed-Mode Bending Method for Delamination Testing *AIAA J* vol 28 no 7 pp 1270–76 DOI: 10.2514/3.25204
[12] ASTM International 2017 ASTM D3039/D3039M-17 Standard Test Method for Tensile Properties of Polymer Matrix Composite Materials DOI: https://doi.org/10.1520/D3039_D3039M-17
[13] Agastra P 2003 Mixed Mode Delamination of Glass Fiber/Polymer Matrix Composites Montana State University
[14] ASTM International 2020 D7079/D7078M-20 Standard Test Method for Shear Properties of Composite Materials by V-Notched Rail Shear Method DOI: https://doi-org.proxybz.lib.montana.edu/10.1520/D7078_D7078M-20

[15] Vintilescu I and Spelt J 1998 Mixed Mode I, II, and III Fracture Characterization of Adhesive Joints *J. Compos. Technol. Res.* DOI: 10.1520/ctr10053j
[16] Broek D and Ric J R 1975 Elementary Engineering Fracture Mechanics *J. Appl. Mech.* DOI: 10.1115/1.3423697